Published in final edited form as:
NMR Biomed. 2012 December ; 25(12): 1321–1330. doi:10.1002/nbm.2804.

Oxygenation in Cervical Cancer and Normal Uterine Cervix assessed using BOLD MRI at 3 T[1]

Rami R. Hallac, **Yao Ding**, **Qing Yuan**, **Roderick W. McColl**, **Jayanthi Lea**[+], **Robert D. Sims**, **Paul T. Weatherall**, and **Ralph P. Mason**

[+]Departments of Radiology and Gynecologic Oncology, University of Texas Southwestern Medical Center, Dallas, TX, USA

Abstract

Hypoxia is reported to be a biomarker for poor prognosis in cervical cancer. However, a practical non-invasive method is needed for routine clinical evaluation of tumor hypoxia. This study examined the potential use of BOLD (Blood Oxygenation Level Dependent) contrast MRI as a non-invasive technique to assess tumor vascular oxygenation at 3 T. Following IRB-approved informed consent and in compliance with HIPAA, successful results were achieved in nine patients with locally advanced cervical cancer (FIGO stage IIA to IVA) and three normal volunteers. In the first four patients, dynamic T_2*-weighted MRI was performed in the transaxial plane using a multi-shot EPI sequence while patients breathed room air followed by oxygen (15 dm^3/min). Later, a multi-echo gradient echo examination was added to provide quantitative R_2* measurements. Baseline T_2*-weighted signal intensity was quite stable, but increased to various extents in tumors upon initiation of oxygen breathing. Signal in normal uterus increased significantly, while iliacus muscle did not change. R_2* responded significantly in healthy uterus, cervix, and eight cervical tumors. This preliminary study demonstrates that BOLD MRI of cervical cancer at 3 T is feasible. However, more patients must be evaluated and followed clinically before any prognostic value can be determined.

Keywords

hypoxia; MRI; cervical cancer; BOLD; oxygen

Introduction

Tumor hypoxia is increasingly recognized as a predictor of malignancy, tumor progression, and response to therapy (1, 2). Several studies using the Eppendorf Histograph needle electrode system for various disease sites have shown that tumor hypoxia was associated with poor prognosis, notably for head and neck cancer, prostate, and lung (3-5). The most extensive studies have been applied to cervical cancer, revealing both extensive hypoxia and more rapid rates of recurrence for large hypoxic tumors in node negative patients (6-8). Patients with recurrent cervical cancers experience dismal survival rates, and thus, there is active interest in developing radiologic imaging methods to identify hypoxia. Preliminary studies using PET following the administration of the hypoxia reporter Cu-ATSM indicate correlation between uptake at 1 hr and progression free survival up to two years (9). Other studies indicate that pharmacokinetic DCE (Dynamic Contrast-Enhanced) CT or MRI

[1]Presented in part at the 18th ISMRM, Stockhlm, Sweden, May 2010.

Correspondence should be addressed: Ralph P. Mason, PhD, Department of Radiology, UT Southwestern Medical Center, 5323 Harry Hines Blvd., Dallas, TX 75390-9058, USA, Phone: +1 (214) 648-8926, Fax: +1 (214) 648-2991, Ralph.Mason@UTSouthwestern.edu.

parameters correlate with hypoxia determined using electrodes in groups of human cervical tumors (10-12). However, DCE approaches measure tumor perfusion rather than oxygenation, and while the two may be interrelated showing population trends, rigorous correlation appears less satisfactory for individuals. Semi quantitative analysis of rat tumors comparing DCE and BOLD showed correlation in some individual tumors, but not others in our hands (13), and lack of correlation was reported for quantitative analysis of mouse tumors by Baudelet *et al.* (14).

Many diverse MR approaches have been demonstrated for the assessment of tumor oxygenation and hypoxia based on NMR, EPR (Electron Paramagnetic Resonance) or hybrid OMRI (Overhauser Magnetic Resonance Imaging) (15, 16). While these methods often provide quantitative measurements of pO_2, they require administration of reporter molecules and are largely restricted to pre-clinical investigations. In this regard proton MRI exploiting BOLD (Blood Oxygen Level Dependent) contrast has attracted increasing interest as a non-invasive indicator of hypoxia based on intrinsic effective transverse relaxation rate (R_2*) or response to breathing hyperoxic gas (ΔSI or ΔR_2*) (17). Paramagnetic deoxyhemoglobin in blood induces transverse relaxation (18, 19), which is the basis of the so-called fMRI exploited widely to assess neuronal activation. It has been suggested that a fast R_2* rate may be directly indicative of tumor hypoxia (extensive deoxyhemoglobin) (20). However, R_2* is also highly dependent on vascular structure or extent (21, 22), local hematocrit, hemorrhage, calcification, and iron deposition in tissue as well as B_0 field inhomogeneity at tissue interfaces (23, 24). Response to a hyperoxic gas breathing challenge provides further insight into tumor vascular oxygenation as revealed by changes in R_2*, local linewidth or contrast in T_2*-weighted images (20-22, 25-28).

Most human cancer studies have employed a hyperoxic gas breathing challenge to induce BOLD contrast, as demonstrated in diverse (17) or specific disease sites, such as prostate (29-31), head and neck (32), brain (33, 34) or breast (35). Multiple pre-clinical studies have explored response to interventions, and sometimes compared BOLD contrast with pO_2 (13, 21, 22, 25-28, 30, 36-43). A recent report showed that a large BOLD response (ΔSI >3%) in the 13762NF rat breast tumor corresponded with elimination of tumor hypoxia (HF_{10}<5%) accompanying oxygen breathing (27).

These reports prompted us to examine the feasibility of adding the BOLD contrast imaging sequence to standard MRI examinations of patients with cervical cancer; we now describe the evolution of a method that is both robust and clinically practical.

Experimental

This study was approved by the Institutional Review Board and complies with the Health Insurance Portability and Accountability Act (HIPAA). Examinations were performed using a 3-T MR scanner (Achieva, Philips Medical Systems, Cleveland, OH) following consent. We evaluated 3 healthy volunteers, and 10 patients: 8 with invasive cervical squamous cell carcinoma (SCC) and 2 with invasive adenocarcinoma (patients 8 and 9). Two of the ten patients were found to have metal clips. Tumor size was estimated from the high resolution MR planning images. The patients' median age was 44 years (range 36 to 56 years) with FIGO stage IIA to IVA. Hematocrit ranged from 33.2% to 41.1% with no obvious trend with respect to disease extent or BOLD response. For the first volunteer and first four patients data were acquired in the transaxial plane as follows:

1. Anatomical high resolution T_2-weighted (T_2-W) images: TR/TE = 6,700/130 ms, FA 90°, FOV = 180 mm, matrix size = 340×309, slice thickness= 4 mm.

2. Axial T_2*-W images during air breathing and oxygen breathing (30 images in 8 mins.): Multiple-Shot EPI was used with the following parameters: TR/TE = 500/41 ms, FA = 70°, FOV = 220 mm, matrix size = 240×240, slice thickness= 5 mm, EPI factor=7, number of averages=2.

For the second and third normal volunteers this approach was attempted in the sagittal plane instead of axial plane.

For the third volunteer and the later patients quantitative R_2* measurements were performed in the sagittal plane. The data were acquired as follows:

1. Anatomical high resolution T_2-W images: TR/TE = 6,700/130 ms, FA = 90°, FOV = 180 mm, matrix size = 340×309, slice thickness = 4 mm.
2. Sagittal T_2*-W images during air breathing (8 images in 2 mins) and oxygen breathing (22 images in 8 mins): based on Multiple-Echo Gradient Echo (MGRE) sequence: TR = 65 ms, FA = 30°, FOV = 300 mm, matrix size = 240×240, thickness = 5 mm, 1 slice. Echo Time (TE) was arrayed with 16 echoes using minimum TE = 2 ms and ΔTE = 2.5 ms to generate the R_2* maps.

Images were acquired using a 6-element SENSE body coil. Patients and volunteers were examined during room air breathing followed by 100% oxygen (15 dm^3/min.), which was administered via a face mask (adult oxygen mask, CareFusion, France) that was worn throughout the experiment. Arterial pressure of oxygen (SaO_2) and heart rate were monitored throughout the experiment using a pulse oximeter (In vivo 4500 MRI, In vivo Research Inc., Orlando, FL).

Data analysis

BOLD MRI data analysis was performed using programs written by us in Matlab (MathWorks Inc., Natick, MA). Regions of interest (ROIs) were determined by a board certified radiologist with over eight years experience in body-MRI. The dynamic multishot EPI sequence allowed the measurement of tumor response to oxygen challenge by calculating changes in signal intensity within the ROI selected for the tumor. Signal intensity change was calculated as:

$$\Delta SI = \frac{SI_t - SI_b}{SI_b} \cdot 100\% \quad (1)$$

where SI_b is the mean baseline signal intensity during air breathing and SI_t is the mean signal intensity with oxygen inhalation. Signal change was also evaluated in the iliacus muscle.

Data acquired using a multi-echo GRE sequence allowed R_2* maps to be generated by fitting the multi-echo T_2*-W image signal intensity to TE, as a single exponential function on a voxel-by-voxel basis:

$$SI = S_0 \cdot e^{-TE \times R_2^*} \quad (2)$$

where SI is signal intensity at each echo time (TE) and S_0 represents a fitted constant. The change of R_2* due to oxygen challenge was then calculated as:

$$\Delta R_2{}^* = R_{2t}{}^* - R_{2b}{}^* \quad (3)$$

where R_{2b}* represents mean baseline rate during air breathing, and R_{2t}* is the mean rate with oxygen inhalation. As a rudimentary comparison with initial studies where only a single echo was acquired, the signal intensity was recorded at the closest time in the multi-echo series (TE = 39 vs. 41 ms earlier) to provide ΔSI. Normal uterine tissue was used as a reference.

Statistical analysis

The mean SI of the T_2*-W images during air breathing was calculated for each ROI and compared with mean SI of the T_2*-W images during oxygen breathing. Initially, we segmented the data into two-minute time increments to assess dynamic changes. We noticed that the response to challenge was significant within 4 minutes after oxygen breathing in seven out of nine patients. However, it was challenging to determine the steady state region for every patient, Therefore, an average of all data points was used to determine the response to challenge. Student's t-tests were performed to examine changes in signal intensity and R_2* response to oxygen breathing ($p < 0.05$ was considered significant).

Results

The ten patients and three normal volunteers tolerated the oxygen breathing challenge without any adverse events. Metal clips adjacent to the cervix of one patient caused severe artifacts and these data were excluded from analysis. In a second patient such artifacts obscured part of the tumor, but the remainder was analyzable. In response to breathing oxygen mean arterial oxygen saturation was found to increase significantly from 97±1 to 99% ($p < 0.05$). Pulse rate ranged from 71 to 99 bpm during baseline air breathing and 64 to 94 with oxygen, which was not significantly different.

Data acquisition was successful in the first volunteer and results are presented for cervix and muscle in Table 1. In the first patient, filling of the bladder displaced the tumor from the selected transaxial imaging plane between the time of initial planning and the oxygen sensitive BOLD contrast study. No further displacement was seen during the BOLD challenge, but the BOLD data were consequently obtained for a slice including only tumor periphery, to which we attribute the particularly large BOLD signal response (ΔSI> 21%, Table 1). Transaxial images obtained using the initial protocol showed well defined anatomy (*e.g.*, Patient #3 in Fig. 1a), allowing regions of interest to be identified in the multi-shot EPI (Fig. 1b). T_2*-weighted signal response (ΔSI) is shown on a voxel-by-voxel basis in the color overlay map (Fig. 1c), revealing considerable heterogeneity in response to oxygen breathing. The signal dynamics are shown for muscle and tumor respectively (Fig. 1d), indicating a significant increase in SI in the tumor upon oxygen challenge (ΔSI = 5.4% ± 3.1%; $p<0.05$), whereas little change was observed in muscle (ΔSI = -0.2±2.5%). The difference is emphasized in the histograms showing voxel-wise distribution of response (Fig. 1e). A significant increase in T_2*-weighted signal was seen in the tumors of all patients (#1-4) evaluated using the EPI approach, while only one patient had a significant change in muscle (Table 1). Sagittal orientation was used for subsequent investigations to compare BOLD response in both the cervical tumor and uterus, and to avoid interference attributed to bladder filling.

Images obtained in the sagittal orientation are shown for the second volunteer with respect to the oxygen challenge (Fig. 2). Anatomy is shown in a central slice allowing regions of interest to be selected. Baseline echo planar images were acquired while the subject breathed ambient room air for 2.5 minutes followed by oxygen. ROIs were selected for normal uterus and cervical tissue (Fig. 2b). Both tissues showed significant signal increase ($p<0.05$) with a much greater signal response in the uterus (ΔSI = 25.4±3.8%) compared to normal cervix (ΔSI = 8.6±2.4%) (Fig. 2 c and d). However, EPI in the sagittal plane failed in volunteer #3,

showing considerable artifacts due to tissue interfaces in the bowel regions. This prompted us to examine the MGRE sequence, which was successful and adopted for the subsequent patients.

Substantial decreases in R_2* rates were found with oxygen breathing in the third healthy volunteer (Fig. 3). Mean signal intensity with respect to successive echoes at different TE values indicated highly consistent data allowing good curve fits to a mono-exponential function (R^2 >0.997, typically) during air and oxygen breathing for both the cervix and uterus (Fig. 3c). Each tissue showed a considerable range of R_2* rates (10 to 50 s^{-1}) and a significant change with oxygen challenge (R_2* = 28.38±1.1 s^{-1} decreased to 24.91±0.8 s^{-1} or ΔR_2* = -12.2% in uterus, and R_2* = 29.47±1.2 s^{-1} decreased to 26.65±0.9 s^{-1} or ΔR_2*= -9.6% in cervix).

The multi echo gradient echo sequence was successfully applied to the subsequent five patients and representative data are shown for patient #8 (Fig. 4). Individual voxels showed R_2* ranging from 10 s^{-1} to 154 s^{-1} with a standard deviation ranging from 3 to 16 in an individual map of R_2* at a single time point during air breathing. Repeated measurements during air breathing showed little variation in mean R_2* rates for individual tumors with standard errors ranging from 0.1 to 0.4 s^{-1} and 0.2 to 0.3 s^{-1} for uterus. Rapid significant increase in signal was observed in both uterus (ΔSI=8.3±1.3%) and in tumor (ΔSI=1.1±1.7%; Fig. 4g), although the response was considerably smaller in tumor. Corresponding R_2* maps and fitted curves for the same ROIs showed that ΔR_2* was faster in uterus (ΔR_2* = -7.1%) than in tumor (ΔR_2* = -1.5%; Fig. 4h). In this patient, muscle showed a small signal response to breathing oxygen (ΔR_2* =1.2%) with rates of R_2*=40.32 s^{-1} (air) and 42.84 s^{-1} (oxygen).

Several past investigations of BOLD response to hyperoxic gas challenge have reported changes in signal intensity only, and thus we compare the semi-quantitative ΔSI with R_2*. Relative change in SI was closely related to relative change in R_2* (R^2>0.88, $p<0.0002$; Fig. 5a) irrespective of tissue. Meanwhile change in R_2* (%ΔR_2*) was related to baseline R_2* for tumor (R^2>0.53) (Fig. 5b), but not uterus (R^2~0.3). Using the MGRE sequence, we were able to calculate the fitted constant (S_0) using equation 2. Change in S_0 ranged from -1% to 0.3% in the tumors and -0.2% to 1.4% in the uterus. Two of the negative tumor S_0 measurements were significant, as well as two positive S_0 changes in the uterus ($p<0.05$).

Noting the progressive dynamic variation in signal and R_2* for tissue, we conducted further analyses based on 2-minute time increments of oxygen challenge. Three tumors showed a significant response within the first two minutes of oxygen breathing; six of eight were significant by 4 minutes and 7 of 8 by 6 or 8 minutes. Since the kinetics were somewhat different, we have provided mean values for the whole oxygen challenge breathing period in Tables 1 and 2.

Discussion

BOLD contrast MRI was successfully accomplished in 9 of 10 patients with cervical cancer and three normal volunteers. The oxygen breathing paradigm was well tolerated and the only imaging failure was due to metal seeds implanted in the cervix for purposes of treatment planning.

We acquired images in the transaxial plane for the initial volunteer and patients, since this has been traditionally favored as the primary imaging plane for crosssectional diagnostic imaging of cervical cancer. Transaxial images generally allow for high resolution imaging to reveal parametrial tumor extension, and they also allow concurrent assessment of nodal involvement. For the BOLD response to oxygen challenge, we imaged a single plane

through a central part of the tumor, as identified by the radiologist during the scanning procedure, so that both central and peripheral regions could be observed. Comparison of the high resolution diagnostic scans with BOLD provided anatomical identification, and muscle tissue was chosen as a reference standard. The iliacus muscle signal was quite stable both during baseline air breathing and in response to oxygen challenge (*e.g.*, Fig. 1d). This coincides with previous observations in humans at 1.5 T, where oxygen breathing generated no response in R_2* in muscle (or liver and spleen), while carbogen elicited a significant response in all three organs (44). Likewise Winter *et al.* reported a lack of response in rabbit paraspinal muscle at 1.5 T with respect to oxygen challenge, though again carbogen induced a change (45). The differential response to these two hyperoxic gases is often attributed to vasoactivity of carbogen, and has been explored extensively with respect to tumorand wound-induced skin angiogenesis (25). The mature vasculature of well perfused muscle may show little response to oxygen. Meanwhile a large response has been reported accompanying the hyperemia in human muscle following constriction and ischemia (46).

Tumor showed distinct heterogeneity, but a significant mean increase in all four patients (Table 1). Three patients showed quite similar signal response (2.7 to 5.4%), whereas patient #1 showed a much larger change. It became clear that the tumor in patient #1 had become displaced from the original imaging planning location. The tumor showed negligible displacement during the oxygen challenge, but the image plane now coincided with the tumor periphery instead of center due to bladder filling. The larger increase in BOLD response in this patient compared to the other three in this group is likely attributable to more extensive vasculature in the periphery as compared to the center. This artifact prompted us to alter the imaging acquisition plane for the later patients.

To date relatively few R_2* tissue rates have been reported at 3 T. We found cervical tumor and normal uterus to have quite similar rates around $R_2^* = 24\ s^{-1}$ (*c.f.* $T_2^* = 42$ ms) (Table 2). By comparison human kidney is reported to have $T_2^* = 47$ ms with a significant response to oxygen breathing ($\Delta T_2^* \sim$ 1-2 ms (47)), as seen in the tissues here. Human skeletal muscle has been reported to have T_2* around 27 ms at 1.5 T when subjects breathed air (unchanged with oxygen) (44). A range of rates has been reported previously at 3 T, *e.g.*, $T_2^* = 20$ - 30 ms in human tibialis anterior muscle and soleus muscle (48), which is very similar to our measurement in the paraspinal muscle (T_2^*=24.8 ms), though a value of $T_2^* =$ 19 ms was reported for calf muscle (46).

Imaging in the sagittal plane avoids issues of displacement due to bladder filling and clearly shows the relationship of normal cervix or cervical tumor to the uterus and vagina. The well-vascularized endometrium provides a useful positive control, which is highly responsive to oxygen challenge (Fig. 2). Echo planar imaging was less satisfactory in the sagittal plane due to signal losses from extensive susceptibility variations in the bowel regions.

For the later patients (#5-10), we implemented a multi-echo gradient echo sequence, which provides R_2*, as opposed to sampling signal intensity changes alone. This should provide further insurance against artifacts, since R_2* distribution may be compared irrespective of motion artifacts, which otherwise could compromise effective signal subtraction. R_2* maps show heterogeneity in both the uterus and normal cervix (*e.g.*, in Fig. 3) with significant decrease in R_2* upon breathing oxygen.

Two patients presented with surgical metal clips. Artifact from the metal clips obscured most of the tumor in patient 7, which made it hard to analyze (data excluded). Patient 5 also had a metal clip artifact that obscured part of the tumor. Nonetheless, a significant drop in R_2* was observed upon breathing oxygen.

The motivation for developing oxygen sensitive MRI of human cervical cancer is provided by strong evidence that hypoxia influences tumor aggressiveness, notably angiogenesis and metastasis, as well as poor response to therapy and shorter recurrence free intervals. Specifically, in cancer of the cervix, several studies based on the Eppendorf Histograph polarographic electrode system, indicated that patients with hypoxic tumors (variously defined as HF_5>50% or median pO_2 less than the population mean) had a poorer clinical outcome. In 1998, Fyles, *et al.*, reported that cervical cancer patients with larger tumors (>5 cm diameter) had significantly poorer disease-free survival (DFS), if the fraction of pO_2 measurements less than 5 torr (~ 670Pa) was greater than 50%, in a study of 74 patients (DFS 12% vs. 65% at 2 years, P = 0.0001) (49). An extended study of 106 patients published in 2002 noted that the predictive value applied only to node negative patients (7) and a follow-up report indicates that stratification based on hypoxia is less relevant after 10 years (50). Nonetheless, hypoxia was clearly associated with short-term disease free survival and this measurement could become a common and useful clinical tool, if accomplished with a simple noninvasive method.

In addition to assessing tumor hypoxia the dynamic response to an intervention may be important. Electrodes are highly invasive and do not conveniently allow repeat dynamic maps, although Aquino-Parsons *et al.* did examine a group of women with respect to hyperoxic gas breathing challenge, comparing the influence of breathing oxygen or carbogen on cervical tumor pO_2 (51). Results indicated that carbogen was more effective at eliminating hypoxia than oxygen, but carbogen is noted to be quite stressful and thus we opted to apply oxygen breathing challenge here. It has been reported that carbogen-light ($98\%O_2/2\%CO_2$) causes lower stress, while retaining the hemodynamic attributes of carbogen (52-54), and this appears worthy of future investigation for BOLD studies. Warming and humidifying the inhaled gas may also be helpful.

BOLD MRI indicates changes in vascular oxygenation, but may be further influenced by flow, vascular volume, pH, R_1 changes, and hematocrit (21, 26). We tested two pulse sequences to acquire BOLD images. Semi-quantitative approaches based on simple changes in T_2-weighted signal intensity are particularly sensitive to flow (21), although this has been applied to many pre-clinical and clinical investigations (13, 17, 26, 38, 43). Use of MGRE to assess R_2* is relatively insensitive to inflow (21) and has been favored in more recent studies (27, 30, 36, 37). It is noteworthy that we observed strong correlation between changes in SI and R_2* (Fig. 5a) suggesting that inflow and R_1 changes are not a major factor in response. Nonetheless, significant changes in S_0 were observed for two tumors and two uteri with respect to oxygen challenge. The S_0 changes may have been caused by changes in R_1 or vascular volume. A correlation was also found between ΔR_2* and baseline R_2* (Fig. 5b), in line with a previous report for chemically induced spontaneous rat breast tumors (36).

Rates of tissue response may also provide useful insight into tumor perfusion and oxygenation. Tumors in Patients #3 and #8, shown in Figures 1 and 4 respectively, showed considerable increase, albeit with minor hiccups, in signal over the whole 8-minute oxygen challenge. Other tumors reached a plateau or maximum at an earlier time.

The EPI sequence is sensitive to susceptibility differences, which result in signal loss, limited spatial resolution, and image distortion. Indeed, we were unable to achieve useful EPI in volunteer # 3 and subsequent studies were performed using MGRE. This has the added bonus of providing both relative signal intensity changes and R_2*. Relative SI changes were larger on the EPI sequence compared to the MGRE. Since different MRI parameters were in both sequences, a direct comparison between relative SI is not feasible.

BOLD response is sensitive to tumor vascular oxygenation as well as the extent of vasculature (21, 22). Measurements of tissue R_1 therefore may be relevant, since they are directly sensitive to changes in pO_2 (55, 56). While there is a small R_1 response to deoxyhemoglobin (57, 58), we believe it will ultimately be useful to implement and evaluate interleaved BOLD and TOLD (Tissue Oxygenation Level Dependent) measurements. Indeed, a preliminary report of well defined rat prostate tumors indicated differential temporal response to T_1- and T_2*-weighted signal, presumably reflecting alteration in vascular oxygenation followed by diffusion of oxygen into the tumor tissues (59). A preliminary report did show significant response in T_1 of cervical squamous carcinoma in response to oxygen breathing at 1.5 T (44). Further development of oxygen sensitive MRI of the cervix may usefully compare different gases, *e.g.*, carbogen (25, 32, 35, 44), implementation of alternative oxygen delivery approaches and masks (60), and various pulse sequences (61, 62). Dynamic contrast enhanced (DCE) MRI following infusion of paramagnetic contrast agents has also been reported to provide insight into tumor hypoxia (10-12). Likewise, histological correlates could provide further insight into the nature of tumor hypoxia and perfusion (63). In our initial protocol described here, emphasis was on optimizing the BOLD study, but including additional methods should be straightforward in the future.

Despite several decades of significant treatment advances for cervical cancer, it remains a prevalent life-threatening disease. As such development of accurate prognostic biomarkers will almost certainly improve and eventually optimize and personalize therapy. This preliminary study demonstrates that BOLD MRI at 3-tesla is feasible for examining the potentially valuable biomarker of oxygenation seen in cervical cancer. It remains to be seen whether baseline R_2*, signal response to hyperoxic gas breathing or a multi parametric comparison including additional parameters such as tumor size, and stage will be most useful. Further parameters such as vascular perfusion and permeability based on DCE, cellularity based on diffusion, and TOLD response to oxygen challenge may also be readily incorporated into a dynamic evaluation. More patients must be evaluated and followed clinically before the prognostic value of this non-invasive technique is determined.

Acknowledgments

We are grateful to Debbie Travalini (PA),Sarah McNeil (RN), Nikita Shah, and Dr. Elyssia Outlaw for logistic assistance.

This research was supported in part by The Mary Kay Ash Foundation and Harold C. Simmons Cancer Center through 1 P30 CA142543.

References

1. Tatum JL, Kelloff GJ, Gillies RJ, Arbeit JM, Brown JM, Chao KS, Chapman JD, Eckelman WC, Fyles AW, Giaccia AJ, Hill RP, Koch CJ, Krishna MC, Krohn KA, Lewis JS, Mason RP, Melillo G, Padhani AR, Powis G, Rajendran JG, Reba R, Robinson SP, Semenza GL, Swartz HM, Vaupel P, Yang D, Croft B, Hoffman J, Liu G, Stone H, Sullivan D. Hypoxia: Importance in tumor biology, noninvasive measurement by imaging, and value of its measurement in the management of cancer therapy. Int J Radiat Biol. 2006; 82:699–757. [PubMed: 17118889]
2. Avni R, Cohen B, Neeman M. Hypoxic stress and cancer: imaging the axis of evil in tumor metastasis. NMR Biomed. 2011; 24:569–581. [PubMed: 21793071]
3. Brizel DM, Sibly GS, Prosmitz LR, Scher RL, Dewhirst MW. Tumor hypoxia adversely affects the prognosis of carcinoma of the head and neck. Int J Radiat Oncol Biol Phys. 1997; 38:285–289. [PubMed: 9226314]
4. Movsas B, Chapman JD, Hanlon AL, Horwitz EM, Greenberg RE, Stobbe C, Hanks GE, Pollack A. Hypoxic prostate/muscle pO_2 ratio predicts for biochemical failure in patients with prostate cancer: preliminary findings. Urology. 2002; 60:634–639. [PubMed: 12385924]

5. Le QT, Chen E, Salim A, Cao HB, Kong CS, Whyte R, Donington J, Cannon W, Wakelee H, Tibshirani R, Mitchell JD, Richardson D, O'Byrne KJ, Koong AC, Giaccia AJ. An evaluation of tumor oxygenation and gene expression in patients with early stage non-small cell lung cancers. Clin Cancer Res. 2006; 12:1507–1514. [PubMed: 16533775]
6. Höckel M, Schlenger K, Aral B, Mitze M, Schäffer U, Vaupel P. Association between tumor hypoxia and malignant progression in advanced cancer of the uterine cervix. Cancer Res. 1996; 56:4509–4515. [PubMed: 8813149]
7. Fyles A, Milosevic M, Hedley D, Pintilie M, Levin W, Manchul L, Hill RP. Tumor hypoxia has independent predictor impact only in patients with node-negative cervix cancer. J Clin Oncol. 2002; 20:680–687. [PubMed: 11821448]
8. Rofstad EK, Sundfor K, Lyng H, Trope CG. Hypoxia-induced treatment failure in advanced squamous cell carcinoma of the uterine cervix is primarily due to hypoxia-induced radiation resistance rather than hypoxia-induced metastasis. Br J Cancer. 2000; 83:354–359. [PubMed: 10917551]
9. Dehdashti F, Grigsby PW, Mintun MA, Lewis JS, Siegel BA, Welch MJ. Assessing tumor hypoxia in cervical cancer by positron emission tomography with 60Cu-ATSM: Relationship to therapeutic response--a preliminary report. Int J Radiat Oncol Biol Phys. 2003; 55:1233–1238. [PubMed: 12654432]
10. Haider MA, Milosevic M, Fyles A, Sitartchouk I, Yeung I, Henderson E, Lockwood G, Lee TY, Roberts TPL. Assessment of the tumor microenvironment in cervix cancer using dynamic contrast enhanced CT, interstitial fluid pressure and oxygen measurements. Int J Radiat Oncol Biol Phys. 2005; 62:1100–1107. [PubMed: 15990015]
11. Loncaster JA, Carrington BM, Sykes JR, Jones AP, Todd SM, Cooper R, Buckley DL, Davidson SE, Logue JP, Hunter RD, West CML. Prediction of radiotherapy outcome using dynamic contrast enhanced MRI of carcinoma of the cervix. Int J Radiat Oncol Biol Phys. 2002; 54:759–767. [PubMed: 12377328]
12. Lyng H, Vorren AO, Sundfor K, Taksdal I, Lien HH, Kaalhus O, Rofstad EK. Assessment of tumor oxygenation in human cervical carcinoma by use of dynamic Gd-DTPA-enhanced MR imaging. J Magn Reson Imaging. 2001; 14:750–756. [PubMed: 11747032]
13. Jiang L, Zhao D, Constantinescu A, Mason RP. Comparison of BOLD contrast and Gd-DTPA Dynamic Contrast Enhanced imaging in rat prostate tumor. Magn Reson Med. 2004; 51:953–960. [PubMed: 15122677]
14. Baudelet C, Cron GO, Gallez B. Correlation between BOLD-MRI and DCE-MRI using P792 in experimental fibrosarcoma tumors. Magn Reson Med. 2006; 56:1041–1049. [PubMed: 16986109]
15. Pacheco-Torres J, López-Larrubia P, Ballesteros P, Cerdán S. Imaging tumor hypoxia by magnetic resonance methods. NMR Biomed. 2011:1–16. [PubMed: 21259366]
16. Gallez B, Baudelet C, Jordan BF. Assessment of tumor oxygenation by electron paramagnetic resonance: principles and applications. NMR Biomed. 2004; 17:240–262. [PubMed: 15366026]
17. Taylor NJ, Baddeley H, Goodchild KA, Powell MEB, Thoumine M, Culver LA, Stirling JJ, Saunders MI, Hoskin PJ, Phillips H, Padhani AR, Griffiths JR. BOLD MRI of human tumor oxygenation during carbogen breathing. J Magn Reson Imaging. 2001; 14:156–163. [PubMed: 11477674]
18. Thulborn KR, Waterton JC, Matthews PM, Radda GK. Oxygenation dependence of the transverse relaxation time of water protons in whole blood at high field. Biochim Biophys Acta. 1982; 714:265–270. [PubMed: 6275909]
19. Ogawa S, Lee TM, Kay AR, Tank DW. Brain magnetic resonance imaging with contrast dependent on blood oxygenation. Proc Natl Acad Sci (USA). 1990; 87:9868–9872. [PubMed: 2124706]
20. Padhani A. Science to Practice: What Does MR Oxygenation Imaging Tell Us about Human Breast Cancer Hypoxia? Radiology. 2010; 254:1–3. [PubMed: 20032129]
21. Howe FA, Robinson SP, McIntyre DJO, Stubbs M, Griffiths JR. Issues in flow and oxygenation dependent contrast (FLOOD) imaging of tumours. NMR Biomed. 2001; 14:497–506. [PubMed: 11746943]

22. Robinson SP, Rijken PF, Howe FA, McSheehy PM, van der Sanden BP, Heerschap A, Stubbs M, Van Der Kogel AJ, Griffiths JR. Tumor vascular architecture and function evaluated by non-invasive susceptibility MRI methods and immunohistochemistry. J Magn Reson Imaging. 2003; 17:445–454. [PubMed: 12655584]
23. Chavhan GB, Babyn PS, Thomas B, Shroff MM, Haacke EM. Principles, Techniques, and Applications of T2*-based MR Imaging and Its Special Applications. Radiographics. 2009; 29:1433–U1272. [PubMed: 19755604]
24. Fernandez-Seara MA, Wehrli FW. Postprocessing technique to correct for background gradients in image-based R-2(*) measurements. Magn Reson Med. 2000; 44:358–366. [PubMed: 10975885]
25. Neeman M, Dafni H, Bukhari O, Braun RD, Dewhirst MW. In vivo BOLD contrast MRI mapping of subcutaneous vascular function and maturation: Validation by intravital microscopy. Magn Reson Med. 2001; 45:887–898. [PubMed: 11323816]
26. Baudelet C, Gallez B. Current issues in the utility of blood oxygen level dependent MRI for the assessment of modulations in tumor oxygenation. Curr Med Imaging Rev. 2005; 1:229–243.
27. Zhao D, Jiang L, Hahn EW, Mason RP. Comparison of ^{1}H blood oxygen leveldependent (BOLD) and ^{19}F MRI to investigate tumor oxygenation. Magn Reson Med. 2009; 62:357–364. [PubMed: 19526495]
28. Al-Hallaq HA, Fan XB, Zamora M, River JN, Moulder JE, Karczmar GS. Spectrally inhomogeneous BOLD contrast changes detected in rodent tumors with high spectral and spatial resolution MRI. NMR Biomed. 2002; 15:28–36. [PubMed: 11840550]
29. Diergarten T, Martirosian P, Kottke R, Vogel U, Stenzl A, Claussen CD, Schlemmer HP. Functional characterization of prostate cancer by integrated magnetic resonance imaging and oxygenation changes during carbogen breathing. Invest Radiol. 2005; 40:102–109. [PubMed: 15654255]
30. Alonzi R, Padhani AR, Maxwell RJ, Taylor NJ, Stirling JJ, Wilson JI, d'Arcy JA, Collins DJ, Saunders MI, Hoskin PJ. Carbogen breathing increases prostate cancer oxygenation: a translational MRI study in murine xenografts and humans. Br J Cancer. 2009; 100:644–648. [PubMed: 19190629]
31. Chopra S, Foltz WD, Milosevic MF, Toi A, Bristow RG, MÃ©nard C, Haider M A. Comparing oxygen-sensitive MRI (BOLD R2*) with oxygen electrode measurements: A pilot study in men with prostate cancer. Int J Radiat Biol. 2009; 85:805–813. [PubMed: 19728195]
32. Rijpkema M, Kaanders JH, Joosten FB, van der Kogel AJ, Heerschap A. Effects of breathing a hyperoxic hypercapnic gas mixture on blood oxygenation and vascularity of head-and-neck tumors as measured by magnetic resonance imaging. Int J Radiat Oncol Biol Phys. 2002; 53:1185–1191. [PubMed: 12128119]
33. Muller A, Remmele S, Wenningmann I, Clusmann H, Traber F, Flacke S, Konig R, Gieseke J, Willinek WA, Schild HH, Murtz P. Intracranial Tumor Response to Respiratory Challenges at 3.0 T: Impact of Different Methods to Quantify Changes in the MR Relaxation Rate R2*. J Magn Reson Imaging. 2010; 32:17–23. [PubMed: 20578006]
34. Muller A, Remmele S, Wenningmann I, Clusmann H, Traber F, Flacke S, Konig R, Gieseke J, Willinek WA, Schild HH, Murtz P. Analysing the response in R_2* relaxation rate of intracranial tumours to hyperoxic and hypercapnic respiratory challenges: initial results. Europ Radiol. 2011; 21:786–798.
35. Rakow-Penner R, Daniel B, Glover GH. Detecting Blood Oxygen Level-Dependent (BOLD) Contrast in the Breast. J Magn Reson Imaging. 2010; 32:120–129. [PubMed: 20578018]
36. McPhail LD, Robinson SP. Intrinsic Susceptibility MR Imaging of Chemically Induced Rat Mammary Tumors: Relationship to Histologic Assessment of Hypoxia and Fibrosis. Radiology. 2010; 254:110–118. [PubMed: 20032145]
37. Rodrigues LM, Howe FA, Griffiths JR, Robinson SP. Tumor R-2 * is a prognostic indicator of acute radiotherapeutic response in rodent tumors. J Magn Reson Imaging. 2004; 19:482–488. [PubMed: 15065173]
38. Elas M, Williams BB, Parasca A, Mailer C, Pelizzari CA, Lewis MA, River JN, Karczmar GS, Barth ED, Halpern HJ. Quantitative tumor oxymetric images from 4D electron paramagnetic

resonance imaging (EPRI): Methodology and comparison with blood oxygen level-dependent (BOLD) MRI. Magn Reson Med. 2003; 49:682–691. [PubMed: 12652539]

39. Baudelet C, Gallez B. How does blood oxygen level-dependent (BOLD) contrast correlate with oxygen partial pressure (pO_2) inside tumors? Magn Reson Med. 2002; 48:980–986. [PubMed: 12465107]
40. Dunn JF, O'Hara JA, Zaim-Wadghiri Y, Lei H, Meyerand ME, Grinberg OY, Hou H, Hoopes PJ, Demidenko E, Swartz HM. Changes in oxygenation of intracranial tumors with carbogen: a BOLD MRI and EPR oximetry study. J Magn Reson Imaging. 2002; 16:511–521. [PubMed: 12412027]
41. Jordan BF, Crokart N, Baudelet C, Cron GO, Ansiaux R, Gallez B. Complex relationship between changes in oxygenation status and changes in R-2(*): The case of insulin and NS-398, two inhibitors of oxygen consumption. Magn Reson Med. 2006; 56:637–643. [PubMed: 16897769]
42. Fan X, River JN, Zamora M, Al-Hallaq HA, Karczmar GS. Effect of carbogen on tumor oxygenation: combined fluorine-19 and proton MRI measurements. Int J Radiat Oncol Biol Phys. 2002; 54:1202–1209. [PubMed: 12419449]
43. Thomas CD, Chenu E, Walczak C, Plessis MJ, Perin F, Volk A. Morphological and carbogen-based functional MRI of a chemically induced liver tumor model in mice. Magn Reson Med. 2003; 50:522–530. [PubMed: 12939760]
44. O'Connor JPB, Naish JH, Jackson A, Waterton JC, Watson Y, Cheung S, Buckley DL, McGrath DM, Buonaccorsi GA, Mills SJ, Roberts C, Jayson GC, Parker GJM. Comparison of Normal Tissue R-1 and R-2* Modulation by Oxygen and Carbogen. Magn Reson Med. 2009; 61:75–83. [PubMed: 19097212]
45. Winter JD, Estrada M, Cheng HLM. Normal Tissue Quantitative T1 and T2(star) MRI Relaxation Time Responses to Hypercapnic and Hyperoxic Gases. Acad Radiol. 2011; 18:1159–1167. [PubMed: 21704536]
46. Lebon V, Carlier PG, Brillault-Salvat C, Leroy-Willig A. Simultaneous measurement of perfusion and oxygenation changes using a multiple gradient-echo sequence: Application to human muscle study. Magn Reson Imaging. 1998; 16:721–729. [PubMed: 9811138]
47. Boss A, Martirosian P, Jehs MC, Dietz K, Alber M, Rossi C, Claussen CD, Schick F. Influence of oxygen and carbogen breathing on renal oxygenation measured by T2*-weighted imaging at 3.0 T. Nmr Biomed. 2009; 22:638–645. [PubMed: 19306339]
48. Schwenzer NF, Martirosian P, Machann J, Schraml C, Steidle G, Claussen CD, Schick F. Aging Effects on Human Calf Muscle Properties Assessed by MRI at 3 Tesla. J Magn Reson Imaging. 2009; 29:1346–1354. [PubMed: 19472391]
49. Fyles AW, Milosevic M, Wong R, Kavanagh MC, Pintilie M, Sun A, Chapman W, Levin W, Manchul L, Keane TJ, Hill RP. Oxygenation predicts radiation response and survival in patients with cervix cancer. Radiother Oncol. 1998; 48:149–156. [PubMed: 9783886]
50. Fyles A, Milosevic M, Pintilie M, Syed A, Levin W, Manchul L, Hill RP. Long-term performance of interstitial fluid pressure and hypoxia as prognostic factors in cervix cancer. Radiother Oncol. 2006; 80:132–137. [PubMed: 16920212]
51. Aquino-Parsons C, Green A, Minchinton Al. Oxygen tension in primary gynaecological tumours: the influence of carbon dioxide concentration. Radiother Oncol. 2000; 57:45–51. [PubMed: 11033188]
52. Powell MEB, Collingridge DR, Saunders MI, Hoskin PJ, Hill SA, Chaplin DJ. Improvement in human tumour oxygenation with carbogen of varying carbon dioxide concentrations. Radiother Oncol. 1999; 50:167–171. [PubMed: 10368040]
53. Baddeley H, Brodrick PM, Taylor NJ, Abdelatti MO, Jordan LC, Vasudevan AS, Phillips H, Saunders MI, Hoskin PJ. Gas exchange parameters in radiotherapy patients during breathing of 2%, 3.5% and 5% carbogen gas mixtures. Br J Radiol. 2000; 73:1100–1104. [PubMed: 11271904]
54. van der Sanden BPJ, Heerschap A, Hoofd L, Simonetti AW, Nicolay K, van der Toorn A, Colier WNJM, van der Kogel AJ. Effect of carbogen breathing on the physiological profile of human glioma xenografts. Magn Reson Med. 1999; 42:490–499. [PubMed: 10467293]
55. Matsumoto K, Bernardo M, Subramanian S, Choyke P, Mitchell JB, Krishna MC, Lizak MJ. MR assessment of changes of tumor in response to hyperbaric oxygen treatment. Magn Reson Med. 2006; 56:240–246. [PubMed: 16795082]

56. O'Connor JPB, Naish JH, Parker GJM, Waterton JC, Watson Y, Jayson GC, Buonaccorsi GA, Cheung S, Buckley DL, McGrath DM, West CML, Davidson SE, Roberts C, Mills SJ, Mitchell CL, Hope L, Ton C, Jackson A. Preliminary Study of Oxygen-Enhanced Longitudinal Relaxation in Mri: a Potential Novel Biomarker of Oxygenation Changes in Solid Tumors. Int J Radiat Oncol Biol Phys. 2009; 75:1209–1215. [PubMed: 19327904]
57. d'Othee BJ, Rachmuth G, Munasinghe J, Lang EV. The effect of hyperoxygenation on T_1 relaxation time *in vitro*. Acad Radiol. 2003; 10:854–860. [PubMed: 12945919]
58. Kershaw LE, Naish JH, McGrath DM, Waterton JC, Parker GJM. Measurement of Arterial Plasma Oxygenation in Dynamic Oxygen-Enhanced MRI. Magn Reson Med. 2010; 64:1838–1842. [PubMed: 20677232]
59. Pacheco-Torres, J.; Zhao, D.; Contero, A.; Peschke, P.; Mason, RP. 16th ISMRM. Toronto, Canada: 2008. DOCENT-Dynamic Oxygen Challenge Evaluated by NMR T_1 and T_2* of Tumors; p. 450
60. Prisman E, Slessarev M, Azami T, Nayot D, Milosevic M, Fisher J. Modified oxygen mask to induce target levels of hyperoxia and hypercarbia during radiotherapy: A more effective alternative to carbogen. Int J Radiat Biol. 2007; 83:457–462. [PubMed: 17538795]
61. Remmele S, Dahnke H, Flacke S, Soehle M, Wenningmann I, Kovacs A, Traber F, Muller A, Willinek WA, Konig R, Clusmann H, Gieseke J, Schild HH, Murtz P. Quantification of the Magnetic Resonance Signal Response to Dynamic (C)O-2-Enhanced Imaging in the Brain at 3 T: R-2* BOLD vs. Balanced SSFP. J Magn Reson Imaging. 2010; 31:1300–1310. [PubMed: 20512881]
62. Mürtz P, Flacke S, Müller A, Soehle M, Wenningmann I, Kovacs A, Träber F, Willinek WA, Gieseke J, Schild HH, Remmele S. Changes in the MR relaxation rate R2* induced by respiratory challenges at 3.0 T: a comparison of two quantification methods. NMR Biomed. 2010; 23:1053–1060. [PubMed: 20963801]
63. Padhani AR, Miles KA. Multiparametric Imaging of Tumor Response to Therapy. Radiology. 2010; 256:348–364. [PubMed: 20656830]

Abbreviations

BOLD	Blood Oxygenation Level Dependent contrast
Cu-ATSM	Copper (II) (diacetyl-bis (N4-methylthiosemicarbazone))
DCE	Dynamic Contrast-Enhanced
DFS	isease-free survival EPI
EPR	Electron Paramagnetic Resonance
HIPAA	Health Insurance Portability and Accountability Act
IRB	Institutional Review Board
MGRE	Multiple-Echo Gradient Echo
OMRI	Overhauser Magnetic Resonance Imaging
ROI	Regions of interest
SCC	squamous cell carcinoma
TOLD	Tissue Oxygenation Level Dependent

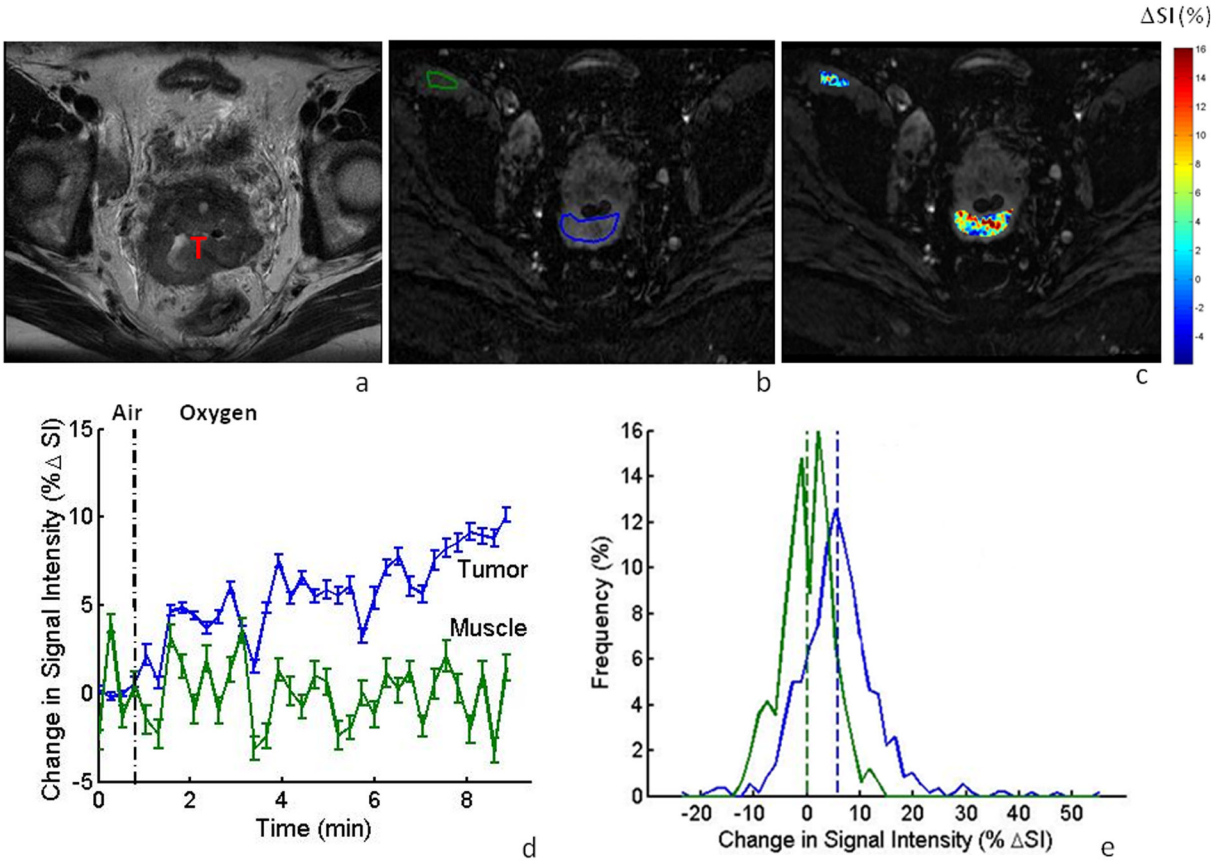

Figure 1. BOLD MRI of cervical tumor in the axial plane

a: High resolution T_2-W image showing cervical tumor (T) for patient #3.

b: T_2*-W image obtained using multi-shot EPI as part of a dynamic data set with ROIs for tumor and iliacus muscle outlined in blue and green, respectively.

c: Maps of %ΔSI for the tumor and muscle overlaid on T_2*-W image, showing heterogeneity of response.

d: Mean tumor signal response to oxygen breathing challenge (ΔSI = 5.4±3.1%) compared to muscle (ΔSI = -0.2±2.5%): vertical bars represent one standard error (SE) at each time point.

e: Distribution of signal changes in tumor (blue) and muscle (green) with oxygen challenge.

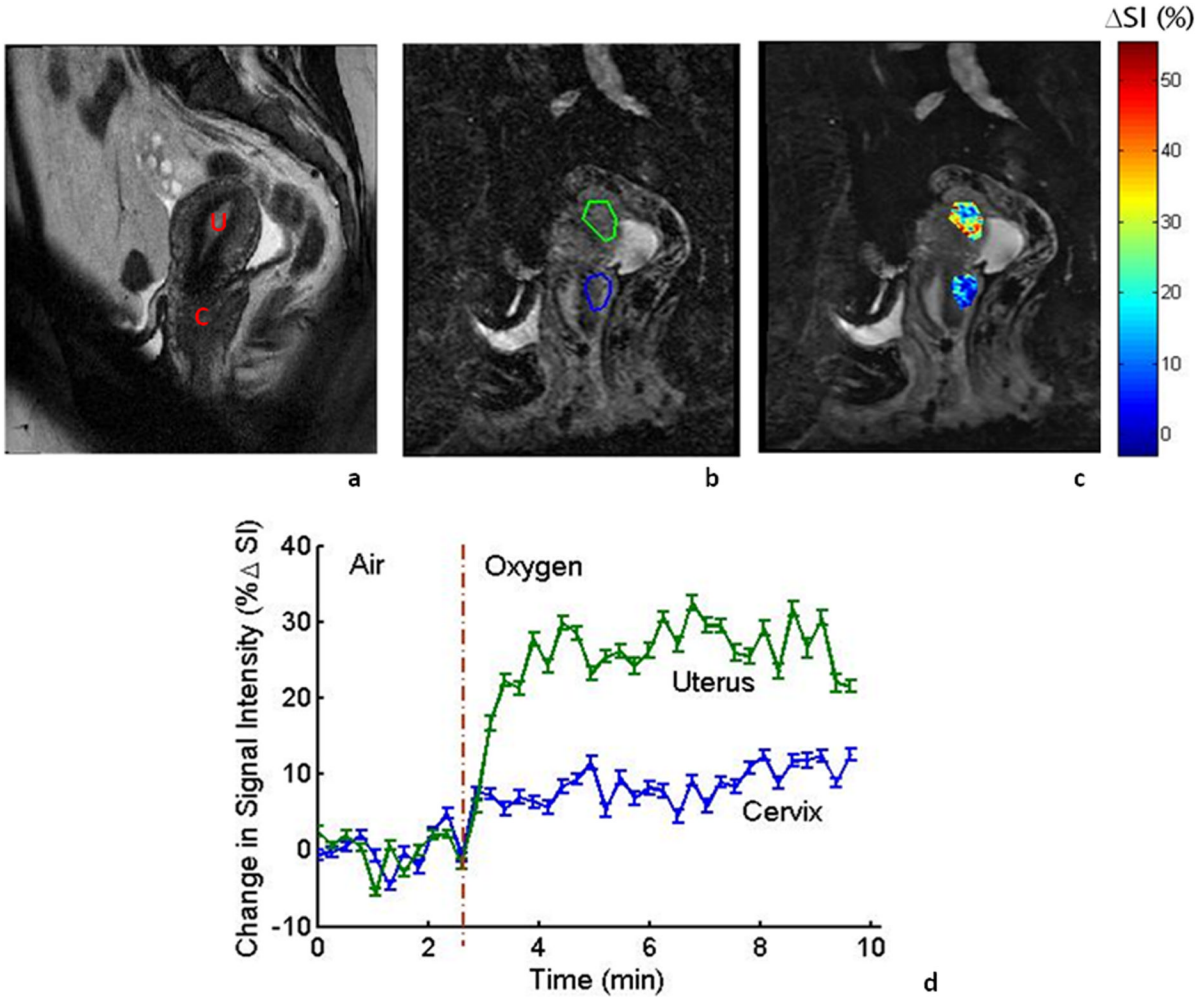

Figure 2. Sagittal imaging in a healthy volunteer with respect to oxygen challenge

a: High resolution T_2-W image showing the cervix (C) and vertically oriented uterus (U) for a normal volunteer (TR/TE = 6.7 s/130 ms, FA=90°, FOV = 180 mm, thickness= 4 mm).

b: T_2*-W image obtained as part of a dynamic data set. ROIs for normal cervical and uterine tissue are outlined in blue and green, respectively. Multiple-Shot Echo Planar Imaging (EPI) used: TR/TE = 500/41 ms, FA = 70°, FOV = 22 cm, thickness= 5 mm.

c: Color maps of %ΔSI in the cervix and uterus overlaid on T_2*-W image.

d: Rapid significant signal response to oxygen breathing was observed in uterus (ΔSI=25.4±3.8%) and cervix (ΔSI=8.6±2.4%). Each point represents mean value ± SE.

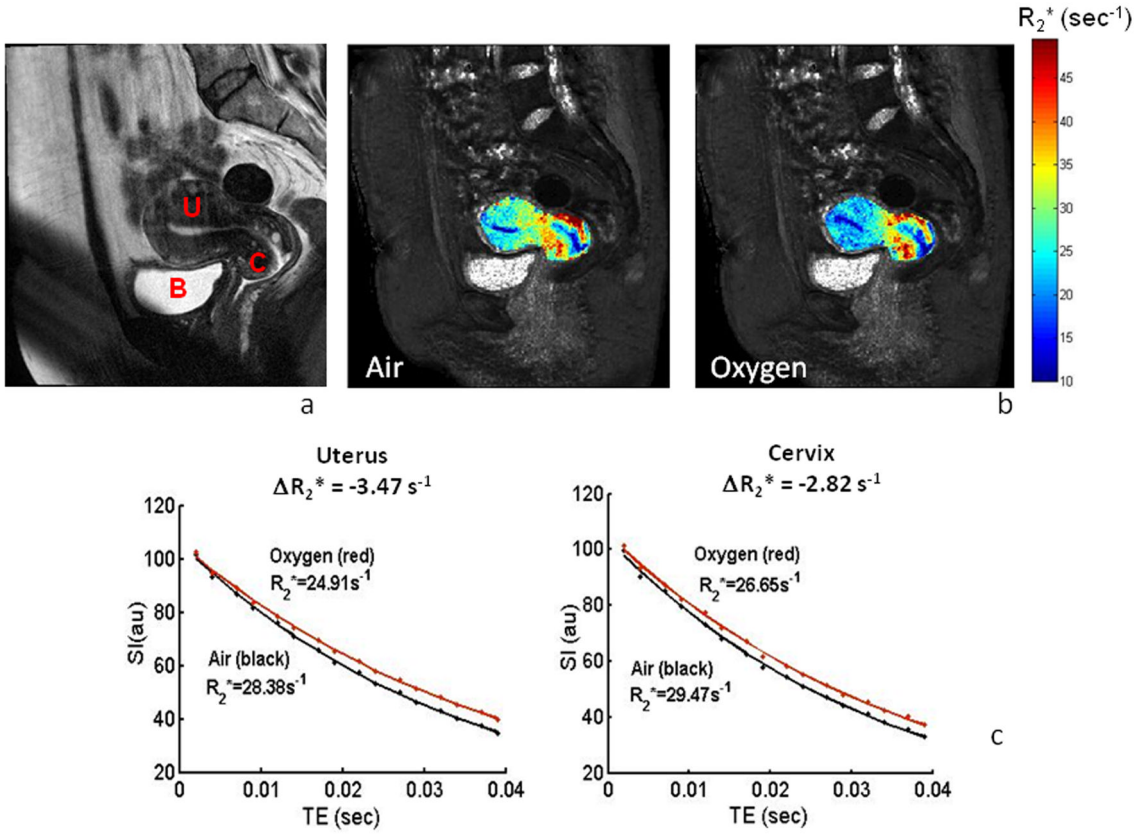

Figure 3. Changes in R_2* in a healthy volunteer

a: High resolution T_2-W image (sagittal) showing the cervix (C) and normally positioned uterus (U) and bladder (B) for normal volunteer #3 acquired using the same parameters as in Figure 2a.

b: R_2* maps of the uterus and cervix overlaid on the T_2*-W GRE image during room-air and oxygen breathing, showing heterogeneity.

c: Variation of mean T_2*-W signal intensity with TE values and mono-exponential fitted curves during air and oxygen breathing for both the cervix and uterus. Normal uterus showed a faster decay rate in R_2* compared to normal cervix with oxygen challenge (quantified as ΔR_2*).

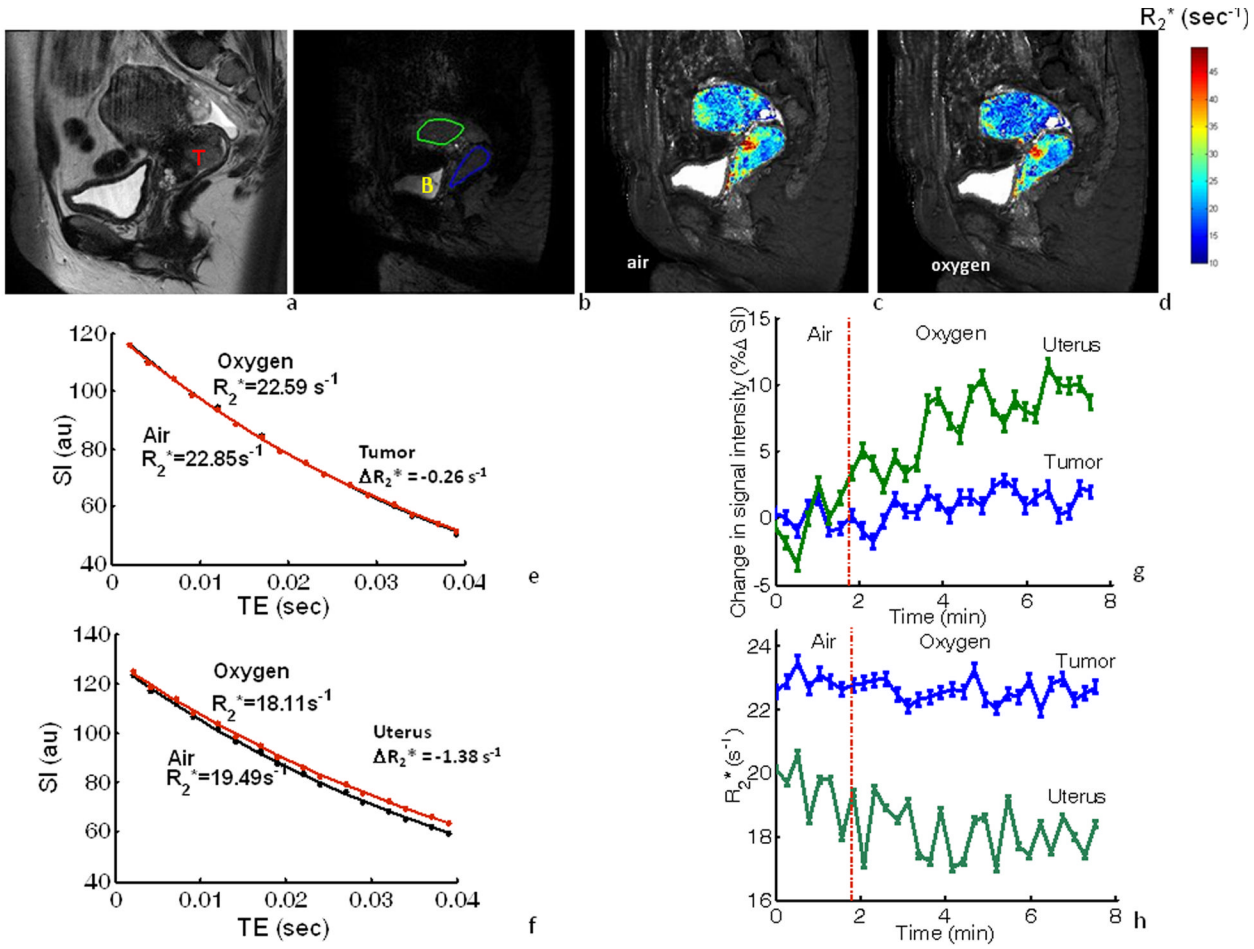

Figure 4. BOLD response to oxygen challenge based on changes in SI and R_2*

a: High resolution T_2-W image (sagittal) showing cervical tumor (T) in patient #8.

b: T_2*-W image obtained as part of a dynamic data set with MGRE imaging. ROIs are shown for tumor (blue) and normal uterus (green); B marks bladder

c-d: R_2* maps of the tumor and uterus overlaid on the T_2*-W image during room-air and oxygen breathing.

e-f: ROI-based T_2*-W signal decay measurements and fitted curves for tumor and uterus while patient breathed air (black) and oxygen (red). Normal uterus showed a faster rate in mean R_2* (ΔR_2*= -1.38 s^{-1}) than tumor (ΔR_2*= -0.26 s^{-1})

g: Variation in mean relative signal response (±SE) obtained from images at TE= 39 ms in MGRE for ROIs identified in b with respect to oxygen breathing challenge. Uterus (green) showed a larger mean signal response to oxygen breathing (ΔSI=8.3±1.3%), compared to tumor (blue; ΔSI=1.1±1.7%).

h: Corresponding R_2* (±SE) for cervical tumor (blue) and uterus (green) with respect to oxygen breathing challenge.

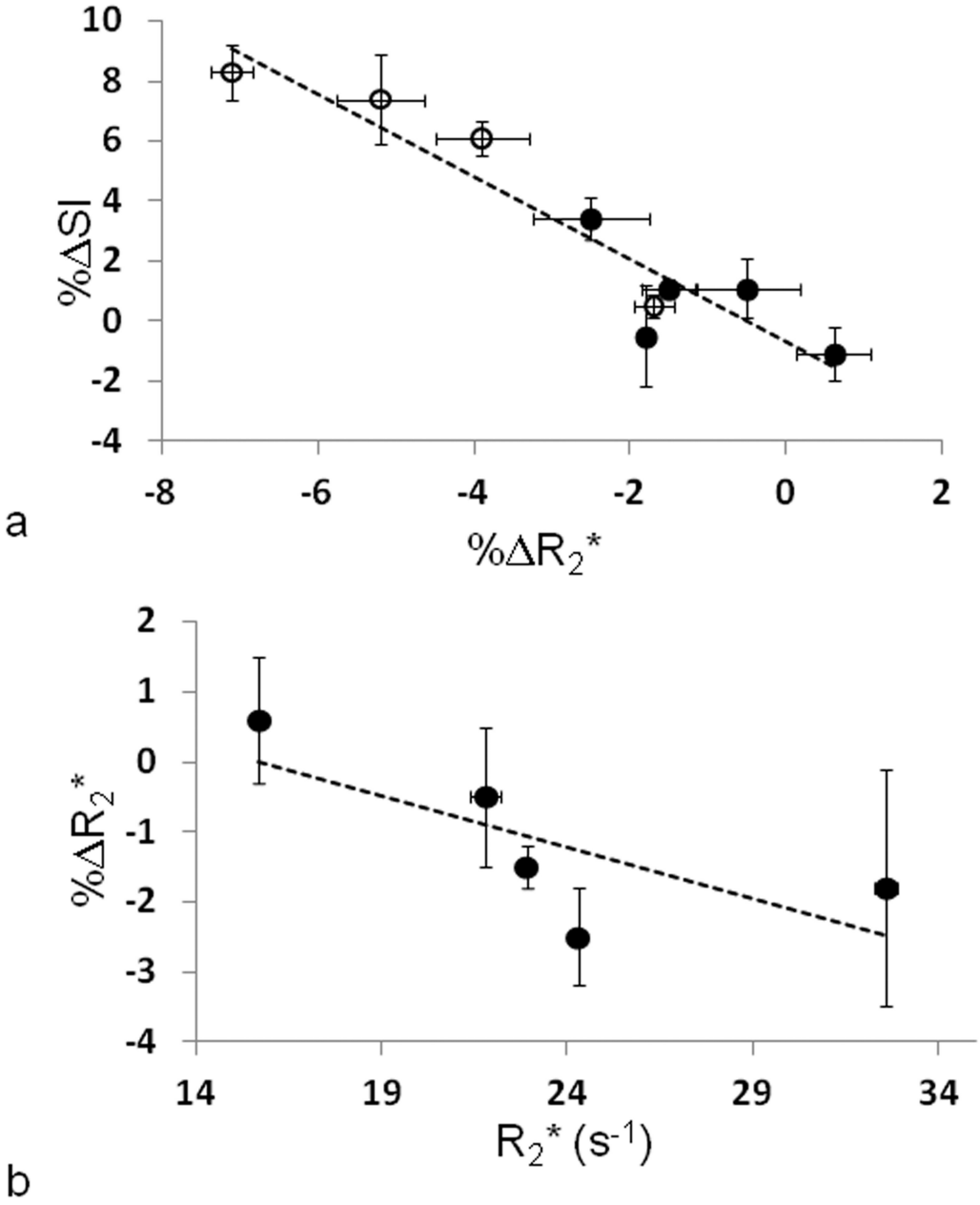

Figure 5. Comparison of semi-quantitative and quantitative BOLD response measurements

a) Relative change in SI accompanying oxygen breathing challenge was closely related to change in R_2* irrespective of tissue (o uterus (n=4); ● cervical tumor (n=5); R^2>0.88, p<0.0002). Data points represent mean ±SE for the whole oxygen challenge period.

b) Change in R_2* (%ΔR_2*) was related to baseline R_2* for the same five tumors shown as ● in (a) (R^2>0.53). Data points represent mean ±SE for the whole oxygen challenge period versus baseline R_2*.

Table 1

BOLD response of cervical tumor, uterus, and iliacus muscle observed in EPI images based on T_2^*-weighted signal response to breathing oxygen

	FIGO Stage	Age	Tumor size	BOLD response (%ΔSI ± SD)		
		years	cm	Tumor	Muscle	
Patient 1	IIIB	47	6.4 *5.5 *5.4	21.2% ± 9.7% † *	0.1% ± 1.9%	
Patient 2	IIB	54	7.2 *6.9 *6.5	3.4% ± 1.7% *	0.1% ± 2.6%	
Patient 3	IIIB	41	6.0 *4.7 *4.6	5.4% ± 3.1% *	-0.2% ± 2.5%	
Patient 4	IVA	38	11.6 *10.2 *8.9	2.7% ± 2.4% *	1.7% ± 5.0% *	
Mean		45		8.1±8.8%	0.4 ± 0.9%	
Normal Volunteer				Cervix	Uterus	Muscle
1	NA			8.2%±2.1% *		-0.5%±1.4%
2 **				8.6%±2.4% *	25.4%±3.8% *	

† signal from tumor periphery

* $p < 0.05$ indicating significant change in signal.

** acquired in the sagittal plane

Table 2

BOLD response of cervical tumor, normal cervix, and uterus observed in the sagittal GRE images based on R_2^* and T_2^*-weighted signal response to breathing oxygen

	FIGO Stage	Age	Tumor size	BOLD response (%ΔSI ± SD)		R_2^* ± SD (s^{-1}) (air/oxygen)		$\%\Delta R_2^*$ ± SD	
		years	cm	Tumor	Uterus	Tumor	Uterus	Tumor	Uterus
Patient 5≠	IIA	48	5.7 *2.8 *2.7	-0.5%±0.5%	0.5%±1.3% *	32.6±0.9 / 32.0±2.8	24.3±0.6 / 23.9±0.5	-1.8% *± 8.7%	-1.7% *± 2.2%
Patient 6	IIB	40	8.6 *7.8 *6.8	-1.1%±2.2%*	N/A	15.7±0.4 / 15.8±0.6	N/A	0.6% *± 4.0%	N/A
Patient 8	IIB	42	3.6 *3.5 *2.9	1.1%±1.7% *	8.3%±1.3%*	22.9±0.3 / 22.6±0.3	19.5±0.9 / 18.1±0.8	-1.5% *± 1.5%	-7.1% *± 4.1%
Patient 9	IIB	36	6.1 *5.6 *4.8	1.1%±2.6% *	7.4%±2.2%*	21.8±1.0 / 21.6±0.8	25.8±0.5 / 24.5±1.5	-0.5%± 3.9%	-5.2% *± 5.8%
Patient 10	IIB	56	7.5 *6.5 *4.3	3.4%±3.5% *	6.1%±2.8%*	24.3±0.6 / 23.7±0.8	28.2±0.5 / 27.1±0.8	-2.5% *± 3.5%	-3.9% *± 2.7%
Mean		44		0.8%±1.6%	5.6%±3.0%	23.5±6.1/ 23.1±5.8	24.5±3.7/ 23.4±3.8	-1.1 % ±1.1%	-4.5% ±2.0%
Normal volunteer 3	NA			Normal cervix 5.7%±1.6%	7.6%± 2.4%	Normal cervix 29.47±1.2/ 26.65±0.9	28.38±1.1/ 24.91±0.8/	Normal cervix -9.6% ± 3.3%	-12.2% ± 4.2%

≠Patient #5 had a metal clip preventing effective analysis of long echo time (TE) images: therefore, the BOLD signal comparison was performed at 17 ms for this patient.

*$p < 0.05$.

N/A: the uterus was poorly recognizable in T_2*-W images of this patient